Investigation of the residual stresses effect on the magnetic properties of CuO nanoparticles synthesized in a low-pressure arc discharge plasma.

I.V. Karpov[1,2], A.V. Ushakov[1,2], V.G. Demin[2], A.A. Shaihadinov[2], A.I. Demchenko[2], L.Yu. Fedorov[1,2,a], E.A. Goncharova[2], A.K. Abkaryan[2]

[1] Federal Research Center Krasnoyarsk Scientific Center of the Siberian Branch of the Russian Academy of Science, 660036, Krasnoyarsk, Russia

[2] Siberian Federal University, Krasnoyarsk, 660041, Russia

a) Author to whom correspondence should be addressed. Electronic mail: 1401-87@mail.ru

Abstract. The laws governing the formation of residual stresses in copper oxide nanoparticles in the process of their direct plasma-chemical synthesis in a low-pressure arc discharge plasma are studied. Correlation dependences of the residual stress and the magnetization of nanoparticles on the pressure of the gas mixture of 10% O_2 + 90% Ar are presented. The problems associated with the bifurcation of the magnetization curves during cooling in zero (ZFC) and non-zero (FC) magnetic field, non-equilibrium behavior, relaxation of magnetization and magnetic viscosity of the obtained CuO nanoparticles are discussed.

Keywords: copper oxide, magnetic properties, residual stresses in nanoparticles

1. Introduction. The study and explanation of the magnetic properties of particles having dimensions in the nanometer range is one of the key tasks in the physics of magnetic materials. Currently, magnetic nanoparticles are widely used as active components of ferrofluids, magnetic particle hyperthermia, information storage media, and also as means of drug delivery for biomedical applications. Antiferromagnetic semiconductor compounds are relatively stable and are characterized by the spatial localization of valence electrons. The paper [1] reports on detailed studies of the magnetization of CuO nanoparticles with a nominal size of 37-6.6 nm. A decrease in particle size is accompanied by the appearance of weak ferromagnetism, and a hysteresis loop. However, the appearance of defects and, as a consequence, the presence of excess charge carriers can lead to a fundamentally different fundamental feature, namely, the phase separation of the system and the appearance of polaron magnetic states in the antiferromagnetic (AF) matrix [2-5]. In this case, the orientation of each moment may change due to competing exchange interactions, for example, near defects in the anion and cation sublattices, or as a result of an incompletely filled coordination shell for surface ions. Thus, the appearance of defects is the main cause of the appearance of ferromagnetism in an antiferromagnetic system, and the size factor is insignificant.

The magnetic properties of nanopowders formed by the plasma-arc method largely depend on the residual stresses in the nanoparticles [6]. Therefore, the development of a method for predicting

the magnitude and sign of residual stresses in nanoparticles is of great theoretical and practical interest. During plasma synthesis of nanoparticles in vacuum, thermal phenomena and residual stresses play the most significant role in the formation of nanoparticles, since the sign and magnitude of the stresses have a great influence on the amount of stored energy in the nanoparticle [7]. These phenomena can be regulated by changing the energy of the condensable particles [8] and get nanoparticles with desired physical properties. To predict the optimal stresses in nanoparticles, both experimental and calculated methods for their determination are used. According to the papers [9, 10], for any plasma synthesis process in vacuum, the main factors affecting the formation of nanoparticles are the energy of the sprayed particles, the condensation temperature, and the residual stresses. Moreover, thermal phenomena and residual stresses play the most significant role in the formation of nanoparticles. Some papers [11, 12] are devoted to the development of methods for determining residual stresses and studying the nature of their formation in structural materials under the influence of various types of processing. An important area is the study of residual stresses in nanoparticles of complex phase and nonstoichiometric composition. The appearance of stresses is also due to the presence of impurities, foreign inclusions, and block boundaries. In view of the above, it is very important to study the nature of thermal stresses arising in plasma-arc powders in the process of their formation. Additional information on the nature of the paramagnetic or frustrated long and short antiferromagnetic order can be provided by local experimental methods.

The purpose of this work is to study the correlation between the processes in the cathode spot of a vacuum arc, the formation of CuO nanoparticles and their anomalous magnetic properties.

2. Experimental. The experimental setup and the dependence of powder properties on spraying conditions are discussed in detail in [13-17]. Argon, which was fed through an evaporator, was used as a plasma-forming gas, and created a base pressure in the chamber. To study the effect of pressure, nanoparticle synthesis was carried out at a base pressure of 10, 60, 120, and 200 Pa. Oxygen was used as the reaction gas. Synthesis of nanoparticles was studied at a flow rate for oxygen of 10 vol.% of the plasma gas supply. Oxygen was supplied to the reactor in such a way as to form a uniform shell around the plasma torch. The morphological composition of the samples was studies on a JEOL JEM-2100 transmission electron microscope. The phase composition of the samples was studied using an Advance D8 X-ray diffractometer in CuK_{α} monochromatic radiation. Quantitative structural-phase analysis of diffractograms was performed using Powder Cell 2.4 full-profile analysis program. PDF4+ databases were used to identify X-ray spectra. X-ray methods are widely used to determine the residual macrostresses [18-20], which are based on the measurement of lattice deformation (δ) under the action of residual macrostresses. The latter, as is well known, lead to a uniform change in the interplanar spacing for the (HKL) planes from do to $d_o + \Delta d$. Therefore

$$\varepsilon = \Delta d/d_0 = \mathrm{ctg}\,\theta_0 \Delta\theta = \mathrm{ctg}\,\theta_0(\theta - \theta_0)$$

The voltage drop across the discharge gap was measured with a pointer device. Magnetic measurements were performed on an MPMS-XL5 magnetometer in the range of magnetic fields up to 60 kOe.

3. Results and discussion. Figures 1 shows the high-resolution transmission electron microscopy images of the obtained nanoparticles. As follows from the results, the obtained powders are strongly agglomerated spherical particles. Particle sizes range from 5 to 20 nm.

The obtained nanoparticles are characterized by high surface energy, which is compensated by their significant aggregation, which causes a significant decrease in the specific surface. Since during the synthesis of nanoparticles in a plasma-chemical reactor, chemical processes always take place, the particle morphology becomes complicated, particles of different chemical composition are formed, mutual diffusion of nanoparticles in the condensed phase, and at a sufficiently high temperature several processes occur simultaneously with the formation of a strong bond between the nanoparticles. With the predominance of layer-by-layer growth of nanoparticles due to the adsorption of atoms and diffusion processes during atomic mass transfer at the interface.

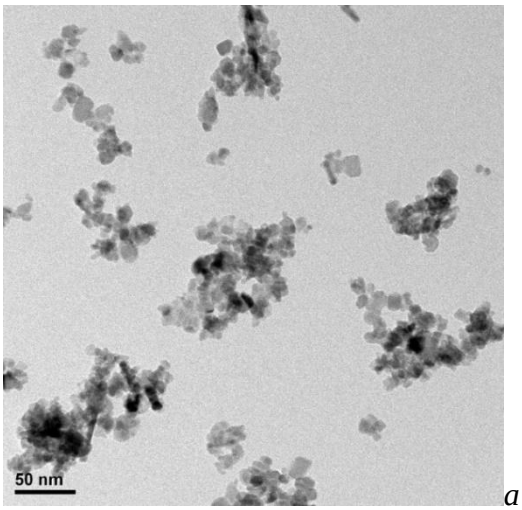

a

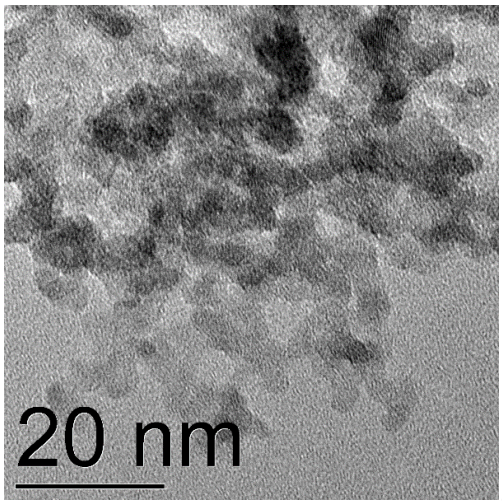

b

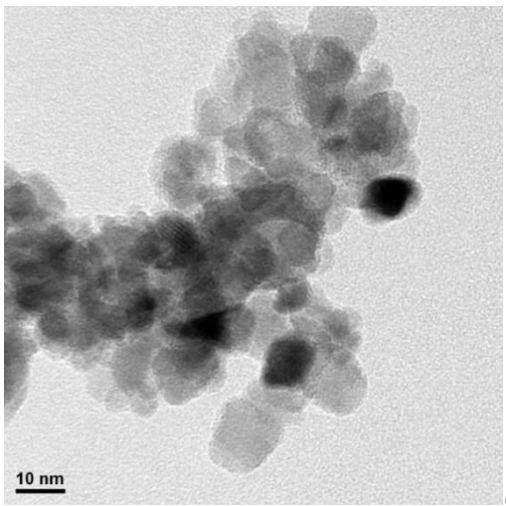

c

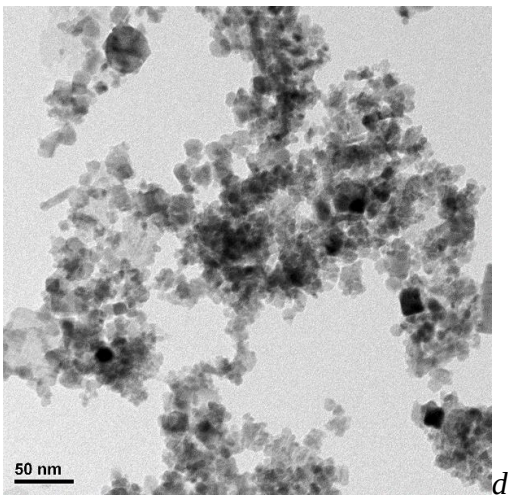

d

Figure 1. TEM images of CuO nanoparticles obtained at a gas mixture pressure of 10 vol.% O_2 + 90% Ar a) 10 Pa b) 60 Pa c) 120 Pa d) 200 Pa. Cathode temperature 300 K.

Figure 2 shows X-ray diffraction patterns of the obtained nanoparticles for values of 2θ in the range from 30 to 80 deg. On the diffractogram of nanoparticles on the background of the X-ray amorphous phase, one can distinguish reflexes (data JCPDS, No. 05-0667) corresponding to the cuprite structure of Cu_2O, space group Pn3m, reflections corresponding to the monoclinic structure of CuO (data JCPDS, No. 45-0937), with lattice parameters a = 4.691 Å, b = 3.432 Å, c = 5.138 Å. There are also reflections with the values 2θ 35.915 °, 44.189 °, 58.396 °, 64.210 °, which apparently correspond to the transition tetragonally distorted cubic crystal lattice of CuO, space group I41 / amd. Two diffraction peaks at 2Θ 43.3 ° and 50.4 ° correspond to the (111) and (200) planes of the face-centered cubic lattice Cu (data JCPDS, no. 04–0836). The presence of unreacted copper nanoparticles is indirectly confirmed by the results of TEM studies. We can see some particles with the color of dark grey. The proportion of CuO relative to other phases, calculated from the most intense lines of the diffraction pattern, is 92% (For pressure 10 Pa). A further increase in the pressure of the gas mixture, according to the diffraction pattern presented, leads to a monotonic increase in the proportion of CuO to 95% (For pressure 60 Pa). No other crystal structures were found. With increasing pressure of the gas mixture, the crystallinity of the nanoparticles decreases. The increase in the share of the X-ray amorphous phase with increasing pressure of the gas mixture is associated with a feature of plasma-chemical synthesis, in which the nanoparticles obtained are saturated with oxygen under thermodynamically non-equilibrium conditions, with a violation of stoichiometry, high residual stresses and a defective crystal structure [21].

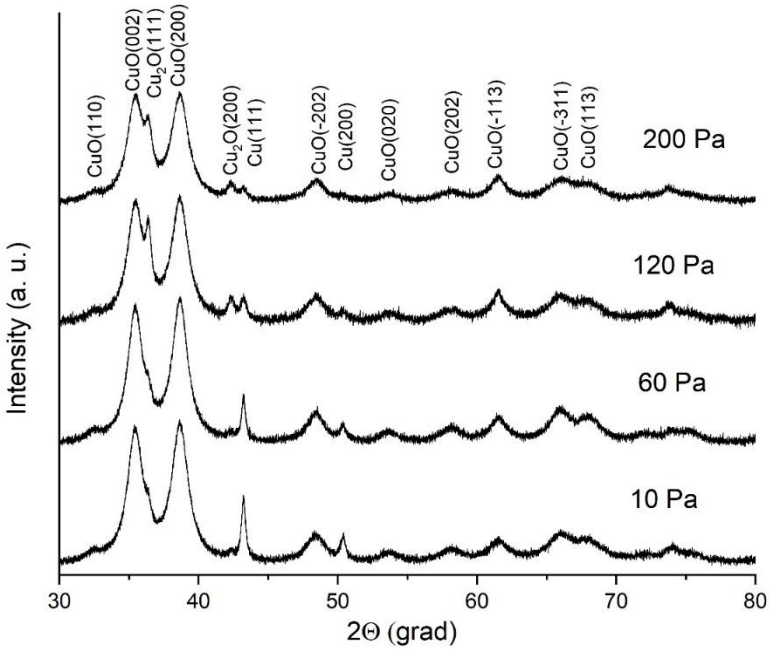

Figure 2. XRD pattern of nanoparticles produced at the different pressure of the gas mixture 10 vol.% O_2 + 90% Ar.

The lattice parameter is slightly less than the standard value (a = 4.6927), which is most likely due to the peculiarities of condensation under reduced pressure. Deformation in particles can be the result of capillary forces, with the largest contribution to the rms displacement is made by static displacements due to the non-uniform nature of deformation in small particles. The lack of completeness of the process of formation of the crystal lattice and, accordingly, an increased concentration of non-equilibrium vacancies due to the abrupt nature of crystallization; the impact of additional surface pressure due to the large contribution of surface energy to the total free energy of small particles, while structural deformations may be non-uniform in particle size. The microstructural characteristics and parameters of the unit cell were determined using the full-profile X-ray analysis using the Rietveld method [22]. Features of the shape of the peaks of the x-ray indicated the presence in the nanoparticles of two fractions differing in size of crystallites. This conclusion was made on the basis of the fact that, with a large integral width, the diffraction maxima had abnormally sharp peaks. Such a complex shape could be explained only by the superposition of two peaks significantly differing in width. Therefore, with a full-profile refinement, two fractions with different crystallite sizes and different percentages were introduced into the model.

Figure 3 presents the results of a study of XRD pattern using PowderCell 2.4.

The dependence of residual stresses on the pressure of the gas mixture is shown. It should be noted that studies have been conducted of the effect of pressure on the magnitude of the residual

stresses of the nanoparticles in a wider range, and only the most significant results are presented in this graph. For example, when the pressure of a gas mixture of 1 Pa and below, the resulting nanoparticles have a very large scatter. To obtain nanoparticles in the pressure range above 200 Pa, in order to maintain a steady arc discharge, it is necessary to increase the voltage, which leads to a transition from a diffuse plasma column to a classical “arched” column, cathode spot bindings and their grouping appear, which leads to splashing of the cathode in the form of large drops.

Figure 3 shows the dependence of the voltage *U* on the discharge gap *d* on the pressure of the gas mixture *p* in the chamber of the plasma-chemical reactor (interelectrode distance *d* has not changed).

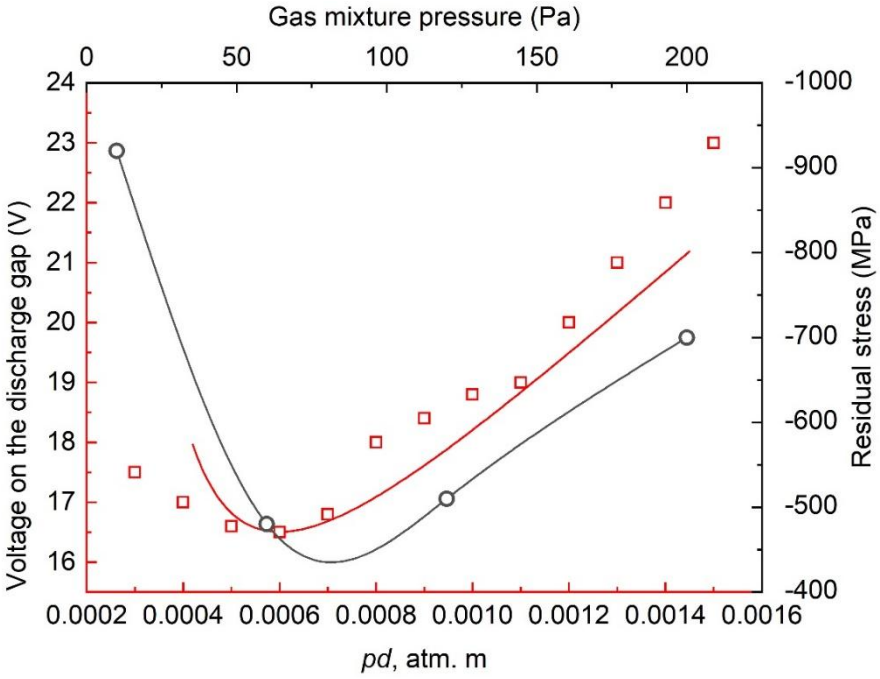

Figure 3. The dependence of the residual stresses of nanoparticles calculated from X-ray diffraction patterns on the pressure of the gas mixture (black line). The dependence of the voltage on the discharge gap of an arc plasma generator with a copper cathode *d* on the pressure *p* of a gas mixture based on argon in a plasma-chemical reactor (red squares) and an approximating curve (red line) calculated from the similarity theory [23].

As can be seen from the figure, the behavior of all the curves is similar: a gradual decrease in the voltage to the inflection point and then an increase up to the maximum value of the pressure of the gas mixture. The behavior of the voltage function curves at the discharge gap is similar in appearance to the dependences of the residual stress in nanoparticles. It should be noted that the measurement of the voltage across the discharge gap in the pressure range of the gas mixture from 10^{-3} Pa to 50 Pa showed an insignificant effect of pressure on plasma and current transfer processes. However, when the pressure of the gas mixture exceeds 50 Pa and up to 200 Pa, there is almost

complete agreement between the behavior of the $U(pd)$ curves and the prediction of the similarity theory.

Since Cu_2O and Cu are weakly diamagnetic and their concentration, according to XRD studies, is insignificant in comparison with CuO, the main contribution to the magnetization is made by the CuO nanoparticles. These differences in residual stresses are also manifested in the nature of the magnetic behavior of CuO nanoparticles. Figure 4 shows the dependence of the magnetic moment $M(H)$ for nanoparticles obtained at different pressures of the gas mixture.

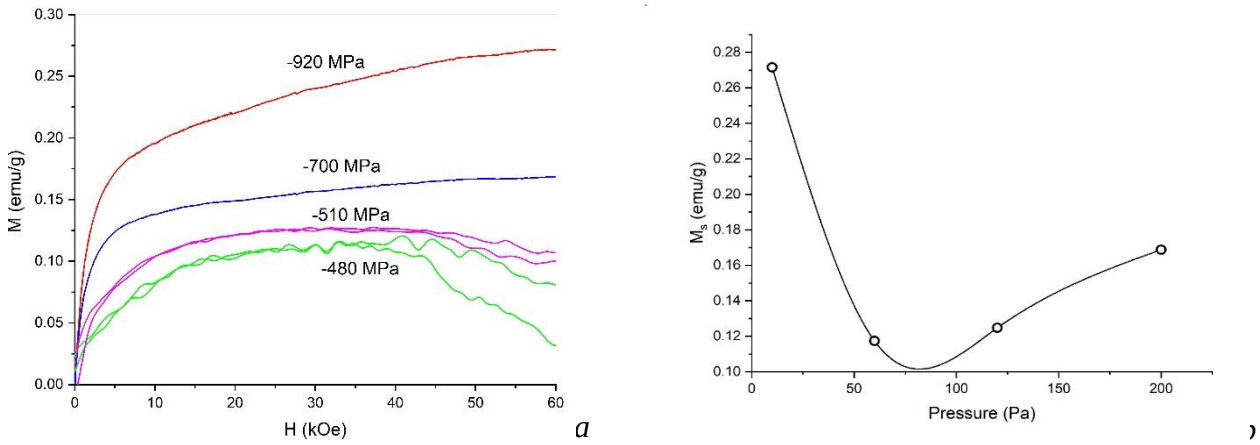

Figure 4 $M(H)$ dependence for nanoparticles obtained at different residual stresses (*a*). Dependence of $M_s(H)$ CuO nanoparticles on the pressure of the gas mixture (*b*).

Based on the observed behavior of CuO nanoparticles, it can be concluded that the magnetic properties of the system under study are related to the magnitude of the residual stresses in the nanoparticles, which, in turn, is related to the processes in the cathode spot of a vacuum arc. Figure 4b shows the dependence of the saturation magnetization of CuO nanoparticles on the pressure of the gas mixture.

The mechanism of the occurrence of residual stresses can be interpreted as follows. Suppose that the forming part of a nanoparticle consists of a large number of clusters, each of which is freely deformed due to the physicochemical processes occurring in it. These deformations are called initial [11]. In real conditions, due to the interaction of the clusters with each other, the initial deformation is constrained; leads to stress. Such stresses (without taking into account thermal stresses) are called crystallization. With further deformation of the system as a result of removing all external influences in the nanoparticle, stresses remain that are residual. The change in energy (pressure in the vacuum chamber) during the deposition (condensation) of nanoparticles leads to thermal expansion of the "nanoparticle-substrate" system. However, due to the presence of a base, different chemical composition (therefore, structure and properties) of the nanoparticle and substrate, as well as a possible temperature gradient over the cross section, thermal expansion is constrained, i.e. there

are tensions. After the end of the nanoparticle formation process on the substrate, the latter is cooled to ambient temperature, which causes stresses associated with the temperature gradient.

The non-stoichiometric composition of the nanoparticles and the presence of several phases have a significant effect on the magnitude of the residual stresses, and this is confirmed by both calculated and experimental data. In particular, for nanoparticles based on copper oxide, the magnitude of compressive stresses increases with decreasing oxygen content in the oxide.

In Figure 5 shows the temperature dependences of the magnetic moment *M(T)* of the obtained CuO nanoparticles during cooling in the field and without the field (ZFC and FC, field 100 Oe) for different pressures of the gas mixture.

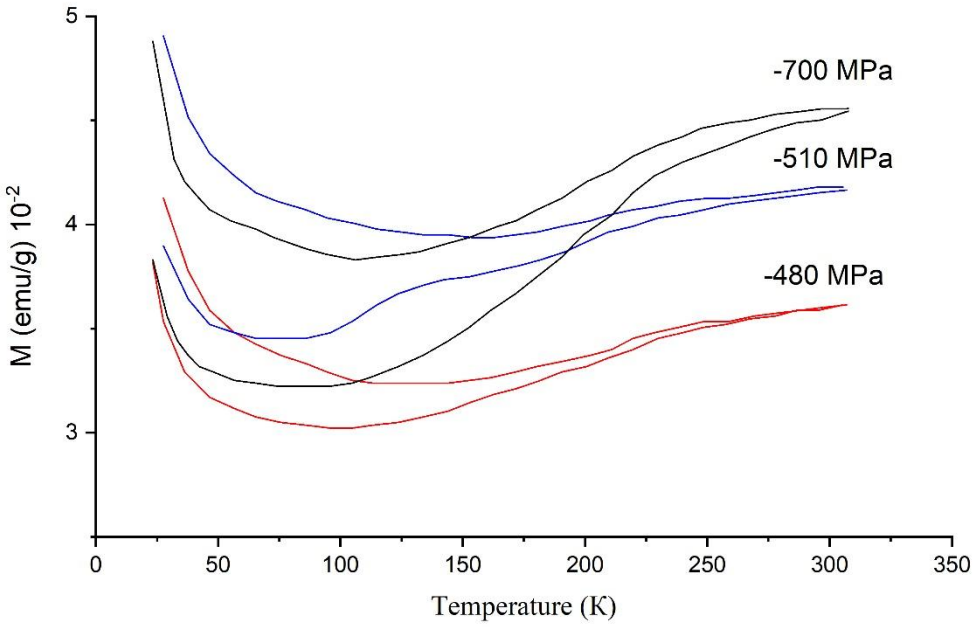

Figure 5 FC and ZFC temperature dependences of the magnetization of nanoparticles obtained at different pressures of the gas mixture in an external field of 100 Oe.

In Figure 5, it can be seen that for as the temperature decreases, the magnetization first decreases and then increases, revealing a clear minimum.

Despite the fact that in ferromagnetic materials, peaks on the ZFC-susceptibility curves should not be observed, however, the disorder inherent in nanoparticles (especially in the near-surface regions) usually leads to disruption of magnetic coupling and the formation of states like spin glass, magnetic clustering in combination with superparamagnetism [24]. The residual stress in the nanoparticles manifests itself in a significant divergence of the *M*(*T*) curves of the ZFC and FC modes, with a clear dependence of the magnitude of the divergence on the residual stress.

Residual stresses can lead to rupture or strengthening of the exchange bonds between the nearest magnetic ions and the violation or the occurrence of long-range magnetic order. In NiO

nanoparticles, an increase in susceptibility was observed with decreasing temperature in the region $T < T_N$, which was associated with the appearance of paramagnetic Ni^{3+} ions [25]. However, it was shown in [26] that the presence of Ni^{3+} ions plays a minimal role in the formation of the magnetic properties of NiO nanoparticles and does not explain the anomalous magnetic properties of nanoparticles.

Figure 6 presents the results of the study of the time dependence of the residual magnetization for nanoparticles obtained at different pressures of the gas mixture.

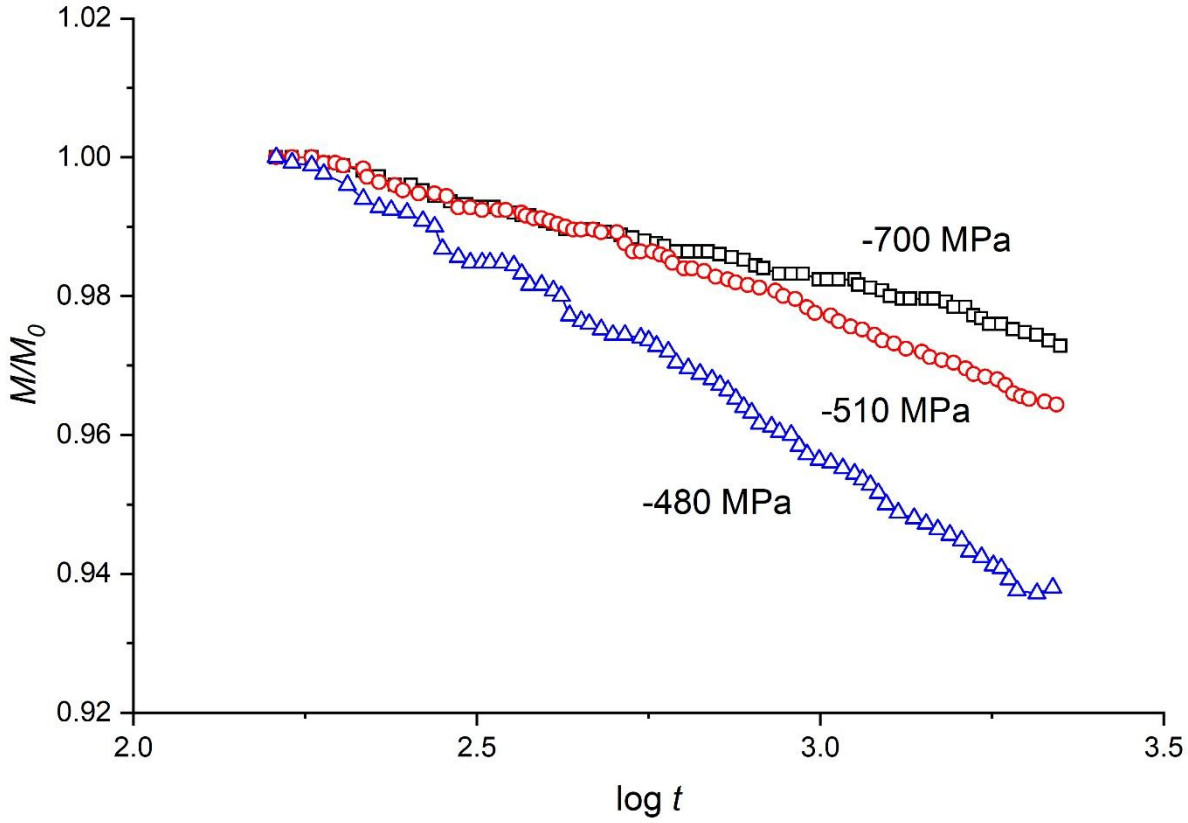

Figure 6. The time dependence of the residual magnetization for nanoparticles obtained at different pressures of the gas mixture.

The data obtained indicate that the ferromagnetic component of all nanoparticles, which appears due to the nonequilibrium state of nanoparticles, is most likely associated with residual stresses in nanoparticles. Any irregularity increases internal energy. The magnetic energy of materials consists of exchange energy, anisotropy energy, magnetoelastic and magnetostatic energies. Changes in these contributions can markedly change the ground magnetic state [27]. When residual stresses appear in the nanoparticles, the degree of symmetry for the surface spins of Cu^{2+} also changes. In a nonequilibrium state, the arrangement of ions both on the surface and in the volume of crystallites becomes not strictly periodic. A local decrease in symmetry leads to an

increase in the magnetic anisotropy energy. Internal elastic stresses due to lattice distortions and an increase in the volume of the unit cell affect the magnetoelastic energy and the change in the exchange energy. The magnetic order in CuO is determined by the competition of various types of magnetic interactions.

Thus, the influence of the technological parameters of nanoparticle synthesis on residual stresses was studied, a correlation was established between the dependence of the magnitude of residual stresses in nanoparticles calculated from XRD pattern, the magnetization of nanoparticles on the pressure of the gas mixture and the dependence of the voltage on the discharge gap of the arc plasma generator on the parameter *pd*, which indicates a single mechanism for the synthesis of nanoparticles in a low pressure arc discharge for a cooled cathode. The observation of the relaxation of the magnetization and magnetic viscosity of the obtained nanoparticles is similar to the behavior demonstrated by other systems of ferromagnetic nanoparticles.

Acknowledgment. The reported study was funded by Russian Foundation for Basic Research (Project No 18-48-242005), Government of Krasnoyarsk Territory, Krasnoyarsk Regional Fund of Science (add. agreement №11/18), to the research project: “Mathematical modeling of interrelated physical processes in dynamic plasma systems of a vacuum arc reactor.”

References

1. A. Punnoose, H. Magnone, M. S. Seehra, Bulk to nanoscale magnetism and exchange bias in CuO nanoparticles, Physical Review B (Condensed Matter and Materials Physics), **64** (2001) 174420, DOI: 10.1103/PhysRevB.64.174420.

2. A.N. Kocharian, Kun Fang, G.W. Fernando, A.V. Balatsky, Phase separation instabilities and magnetism in two dimensional square and honeycomb Hubbard model, Journal of Magnetism and Magnetic Materials **383** (2015) 8-12. https://doi.org/10.1016/j.jmmm.2014.10.007.

3. P.A. Igoshev, M.A. Timirgazin, V.F. Gilmutdinov, A.K. Arzhnikov, V.Yu. Irkhin, Spiral magnetism in the single-band Hubbard model: the Hartree–Fock and slave-boson approaches, Journal of Physics: Condensed Matter **27** (2015) 446002. https://doi.org/10.1088/0953-8984/27/44/446002

4. B.Kh. Khannanov, V.A. Sanina, E.I. Golovenchits, M.P. Scheglov, Electric polarization induced by phase separation in magnetically ordered and paramagnetic states of RMn$_2$O$_5$ (R=Gd, Bi), Journal of Magnetism and Magnetic Materials **421** (2017) 326-335. https://doi.org/10.1016/j.jmmm.2016.08.040.

5. R.F. Mamin, T.S. Shaposhnikova, V.V. Kabanov, Phase separation and second-order phase transition in the phenomenological model for a Coulomb-frustrated two-dimensional system, Phys. Rev. B **97** (2018) 094415. https://doi.org/10.1103/PhysRevB.97.094415.

6. D. Lisjaka, A. Mertelj, Anisotropic magnetic nanoparticles: A review of their properties, syntheses and potential applications, Progress in Materials Science **95** (2018) 286-328. https://doi.org/10.1016/j.pmatsci.2018.03.003.

7. R. Schiedung, I. Steinbach, F. Varnik, Multi-phase-field method for surface tension induced elasticity, Phys. Rev. B **97** (2018) 035410. https://doi.org/10.1103/PhysRevB.97.035410.

8. Dieter Vollath, Franz D. Fischer, D. Holec Beilstein, J. Nanotechnol. **9** (2018) 2265-2276. doi:10.3762/bjnano.9.211.

9. Donald M. Mattox, Handbook of Physical Vapor Deposition (PVD) Processing Book. 2nd Edition. 2010. Elsevier Inc.

10. H.N.G Wadley, X. Zhou, R.A. Johnson, M. Neurock, Mechanisms, models and methods of vapor deposition, Progress in Materials Science **46** (2001) 329-377. https://doi.org/10.1016/S0079-6425(00)00009-8.

11. F.D. Fischer, T. Waitz, D. Vollath, N.K. Simha, On the role of surface energy and surface stress in phase-transforming nanoparticles, Progress in Materials Science **53** (2008) 481-527. doi: 10.1016/j.pmatsci.2007.09.001.

12. D. Tokozakura, R. Nakamura, H. Nakajima, J.G. Lee, H. Mori, Transmission electron

microscopy observation of oxide layer growth on Cu nanoparticles and formation process of hollow oxide particles, Journal of Materials Research **22** (2007) 2930-2935. doi: 10.1557/jmr.2007.0362.

13. I.V. Karpov, A.V. Ushakov, A.A. Lepeshev, L.Yu. Fedorov, Plasma-Chemical Reactor Based on a Low-Pressure Pulsed Arc Discharge for Synthesis of Nanopowders, Technical Physics **62** (2017) 168-173. doi: 10.1134/S106378421701011X.

14. A.V. Ushakov, I.V. Karpov, A.A. Lepeshev, Influence of the Oxygen Concentration on the Formation of Crystalline Phases of TiO_2 during the Low-Pressure Arc-Discharge Plasma Synthesis, Technical Physics **61** (2016) 260-264. doi: 10.1134/S1063784216020262.

15. A.A. Lepeshev, I.V. Karpov, A.V. Ushakov, L.Yu. Fedorov, A.A. Shaikhadinov, Synthesis of Nanosized Titanium Oxide and Nitride Through Vacuum Arc Plasma Expansion Technique, International Journal of Nanoscience **15** (2016) 1550027. doi: http://dx.doi.org/10.1142/S0219581X15500271.

16. L.Yu. Fedorov, I.V. Karpov, A.V. Ushakov, A.A. Lepeshev, Influence of Pressure and Hydrocarbons on Carbide Formation in the Plasma Synthesis of TiC Nanoparticles, Inorganic Materials **51** (2015) 25–28. doi: 10.1134/S0020168515010057.

17. A.V. Ushakov, I.V. Karpov, A.A. Lepeshev, Influence of the Oxygen Concentration on the Formation of Crystalline Phases of ZrO_2 Nanoparticles during the Low-Pressure Arc-Discharge Plasma Synthesis, Physics of the Solid State **57** (2015) 2320–2322. doi: 10.1134/S1063783415110359.

18. H. Ljungcrantz, L. Hultman, J.E. Sungren, Ion induced stress generation in arc-evaporated TiN films, Journal of Applied Physics **78** (1995) 832-837. https://doi.org/10.1063/1.360272.

19. J.A. Sue, Development of arc evaporation of non-stoichiometric titanium nitride coatings, Surface and Coatings Technology **61** (1993) 115–120. https://doi.org/10.1016/0257-8972(93)90212-7.

20. Yu.D. Yagodkin, S.V. Dobatkin, Application of electron microscopy and X-Ray structural analysis for the determination of sizes of structural elements in nanocrystalline materials, Inorg Mater **44** (2008) 1520. https://doi.org/10.1134/S0020168508140070.

21. L.Yu. Fedorov, I.V. Karpov, A.V. Ushakov, A.A. Lepeshev, Study of Phase Composition of CuO/Cu_2O Nanoparticles Produced in the Plasma of a Low-Pressure Arc Discharge, Inorganic Materials: Applied Research. 9 (2018) 323-328. doi: 10.1134/S2075113318020107.

22. H.M. Rietveld, A Profile Refinement Method for Nuclear and Magnetic Structures, J. Appl. Cryst. **2** (1969) 65-71.

23. Friedrich Paschen (1889). "Ueber die zum Funkenübergang in Luft, Wasserstoff und Kohlensäure bei verschiedenen Drucken erforderliche Potentialdifferenz". Annalen der Physik und Chemie. **273** (5): 69-96. DOI:10.1002/andp.18892730505.

24. A.A. Lepeshev, A.V. Ushakov, I.V. Karpov, D.A. Balaev, A.A. Krasikov, A.A. Dubrovskiy, D.A. Velikanov, M.I. Petrov, Particularities of the magnetic state of CuO nanoparticles produced by low-pressure plasma arc discharge, Journal of Superconductivity and Novel Magnetism **30** (2017) 931-936. doi: 10.1007/s10948-016-3885-4.

25. F. Davar, F. Zeinab, M. Salavati-Neyasari, Nanoparticles Ni and Nio: Synthesis, Characterization and magnetic Properties, Journal of Alloys and Compounds **476** (2009) 797-801. http://dx.doi.org/10.1016/j.jallcom.2008.09.121.

26. M. Tadic, D. Nikolic, M. Panjan, G.R. Blake, Magnetic properties of NiO (nickel oxide) nanoparticles: Blocking temperature and Neel temperature, Journal of Alloys and Compounds **647** (2015) 1061-1068. https://doi.org/10.1016/j.jallcom.2015.06.027.

27. S. Thota, J.H. Shim, M.S. Seehra, J. Appl. Phys. **114** (2013) 214307. doi:10.1063/1.4838915.